NMR and *ab initio* study of gallium metal under pressure

R. Řezníček,[1,*] V. Chlan,[2] and J. Haase[1]

[1]*Faculty of Physics and Earth Sciences, University of Leipzig, Linnéstrasse 5, D-04103 Leipzig, Germany*

[2]*Faculty of Mathematics and Physics, Charles University, V Holešovičkách 2, 180 00 Prague 8, Czech Republic*

(Received 28 June 2018; revised manuscript received 27 February 2019; published 15 March 2019)

Gallium metal possesses a complex phase diagram and it has been the subject of many experimental and theoretical studies. Nevertheless, hyperfine properties of its phases requiring higher pressure beyond the liquid-I-II triple point were seldom examined. In this work, hyperfine parameters of liquid and solid gallium metal under pressure are investigated by nuclear magnetic resonance (NMR) measurements and *ab initio* calculations. The electric field gradient and NMR shift of the Ga-III phase are both measured and calculated and their relation to electronic structure is interpreted. Further, calculations of pressure dependencies of the hyperfine parameters of several other solid gallium phases are presented.

DOI: 10.1103/PhysRevB.99.125121

I. INTRODUCTION

Gallium exhibits a complex phase-temperature (P-T) diagram comprising a variety of metastable phases [1,2]. Thus, it generally presents a great opportunity to explore the effects of pressure, temperature, and crystal structure for the physical properties of different phases of the same metallic element. Many experimental results concerning structure determination and phase transition identification [1–10] were published. Various studies focused on other properties including, e.g., elastic properties, phonon dispersion, or the behavior of Ga clusters and superconductivity of gallium [11–22]. The Ga element was also the subject of numerous theoretical investigations [23–40].

The chemical and electronic properties of gallium metal under pressure are rather complex and nuclear magnetic resonance (NMR) may significantly help to understand both. Indeed, there were several NMR or nuclear quadrupole resonance (NQR) studies of liquid gallium [41–49] and of the α-Ga (i.e. Ga-I) [50–58] and β-Ga [58–61] solid phases carried out. However, with the only exception of Ref. [62], the papers on hyperfine properties of gallium metal do not cover phases requiring higher pressure (i.e., well above 1.25 GPa to get beyond the liquid-I-II triple point). Thus, this work takes advantage of the anvil-cell-based high-pressure NMR technique and focuses on NMR experiments on liquid and solid gallium under a pressure up to about 2 GPa at room temperature. The measurements are complemented with *ab initio* calculations of electronic and hyperfine structure of solid gallium, allowing for a corroboration of experimental results and a deeper insight into electronic structure.

II. EXPERIMENT

A. Experimental method

The high-sensitivity NMR anvil pressure cell [63] consisting of a piston and a cylinder made of titanium was fitted with moissanite anvils with a culet diameter of 1.0 mm. A beryllium copper gasket with a 0.5 mm hole contained an RF microcoil of about 300 μm (inner) diameter and 5 turns wound from 25 μm copper wire with 5 μm insulation. A drop of approximately 200 μm of liquid gallium (6N purity level, supplied by ESPI Metals) was placed in the coil together with a ruby chip (coated with cryogenic varnish to avoid any undesired reaction with the gallium sample) serving as a pressure gauge. The cell was then filled with parafine oil used as a pressure medium and external pressure was applied. Care was taken to ensure hydrostatic conditions in the pressure cell by the appropriate choice of the pressure medium and by minimizing the risk of squeezing the gallium sample directly by the culets of the anvils. The pressure was monitored using a laser spectrometer by observing a shift of the R_1 ruby luminescence line [64–66].

At first, only small pressure was applied, so the first experiments were performed under nearly ambient pressure. Next, the pressure in the sample space was increased to 1.15(5) GPa. In the final step, the pressure on the sample reached 2.15(5) GPa and the gallium sample became solid. Most probably (see below) the sample crystallized into the Ga-III phase with body-centered-tetragonal $tI2$ structure [1], which is metastable in this region and can be typically obtained by this approach [1,8]. The stable phase in this P-T region is Ga-II with a complex orthorhombic structure [8] (earlier described as body-centered-cubic [1]), but it requires a different procedure to prepare. One should also consider the metastable monoclinic β-Ga phase [5], although its existence is relatively unlikely under these conditions. The location of the investigated pressure-temperature points in the phase diagram is illustrated in the Supplemental Material [67].

The pressure cell with the sample was installed in a home-made wide-bore NMR probe. The NMR experiments were carried out in a 9.4 T cryomagnet using a phase-coherent spectrometer. The ^{69}Ga and ^{71}Ga isotopes (both with 3/2 spin) were observed. Resonance frequencies of ^{69}Ga and ^{71}Ga nuclei in a reference $Ga(NO_3)_3/D_2O$ solution were

*Richard.Reznicek@physik.uni-leipzig.de

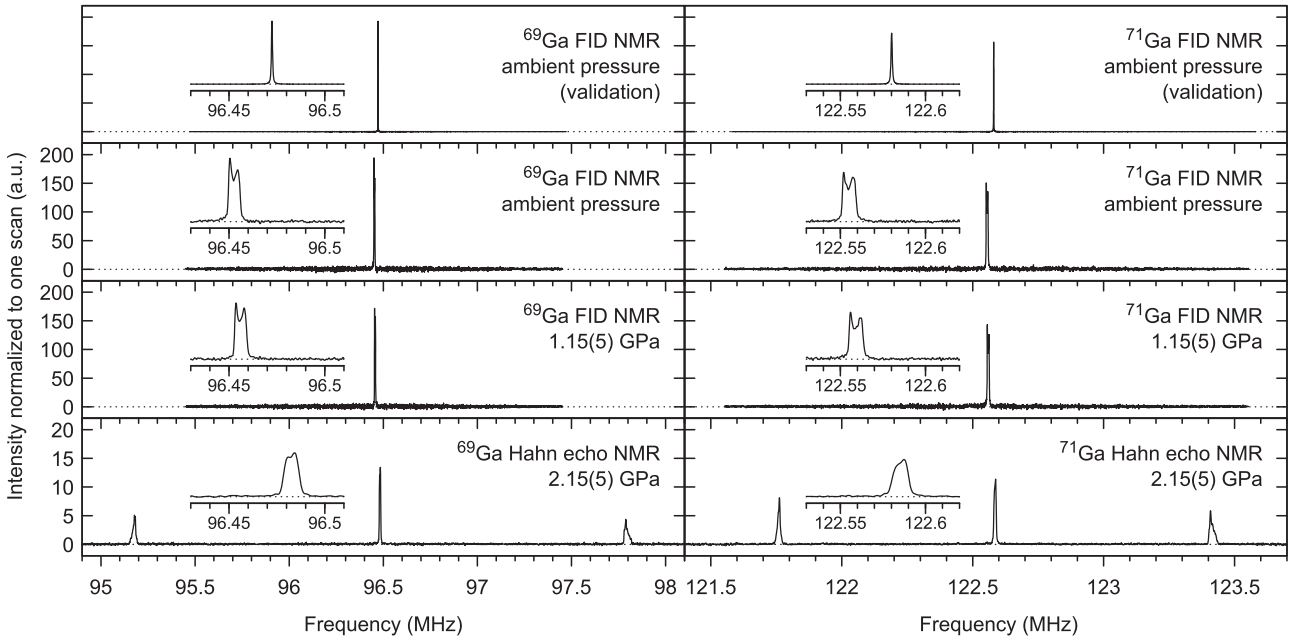

FIG. 1. The NMR spectra of both isotopes of gallium recorded at room temperature for three different pressures. The insets show details of central parts of the spectra.

$^{69}f_{\mathrm{ref}} = 96.04159$ MHz and $^{71}f_{\mathrm{ref}} = 122.03277$ MHz, respectively. The quadrupole moments of the gallium nuclei are $^{69}Q = 17.1(2)$ fm^2 for ^{69}Ga and $^{71}Q = 10.7(1)$ fm^2 for ^{71}Ga [68]. Single-pulse (FID) and Hahn echo pulse sequences were employed for spectra measurements. The relaxation times were determined using the inversion recovery and Hahn echo experiments. The population transfer sequence for detecting shared Zeeman levels consisted of an inversion pulse at satellite frequency immediately followed by the Hahn echo pulse sequence at the central transition frequency. Pulse power of up to 1 W was in most cases sufficient for the microcoil and the pulse duration was adjusted to avoid undesired excitation of neighboring transitions whenever possible, resulting in pulse lengths of several μs. The typical number of scans was on the order of 10^3 to 10^4 for the liquid phase and on the order of 10^5 to 10^6 for the solid phase.

For validation experiments under ambient conditions, a plastic foam (approximately $14 \times 3 \times 1.5$ mm) soaked with gallium metal (the same as above) and wrapped in polyethylene foil was used as a sample. The coil of 10 turns was wound from insulated 0.3 mm copper wire around the sample. The coil with the sample was then installed in the NMR probe instead of the pressure cell and its holder. The pulse sequence consisted of a single pulse (110 W, 5 μs for ^{71}Ga, 7 μs for ^{69}Ga) with a repetition time of 1 s (to avoid heating of the sample) and 512 scans.

B. Experimental results

The NMR spectra of both isotopes in liquid and solid gallium are provided in Fig. 1. Each of the liquid phase spectra (the second and third row in Fig. 1) consists of a single resonance signal [full width at half maximum of ≈67 ppm (≈8.2 kHz) for ^{71}Ga and ≈65 ppm (≈6.2 kHz) for ^{69}Ga] exhibiting a small splitting [≈47 ppm (≈5.7 kHz) for ^{71}Ga and ≈43 ppm (≈4.2 kHz) for ^{69}Ga]. Once the the pressure was increased to 2.15(5) GPa, the sample turned into a solid crystalline phase manifested by a quadrupole split spectrum typical for single crystals; see the lowest panels of Fig. 1. The linewidth of the central transition became a bit bigger than (while still comparable with) the width of the signal observed in the liquid. The central transition splitting was similar to the one of the resonance line in the liquid. The integral intensity of each of the satellites was about 80% of the central transition integral intensity, which can be explained by slightly suboptimal excitation and detection conditions at the satellite frequencies as the probe was tuned to the central transition frequency. In order to verify that the side peaks are indeed satellite signals, a population transfer experiment was performed: an inversion pulse applied at satellite frequency resulted in a significant increase of signal detected by subsequent Hahn echo sequence at the central transition frequency, which meets the expectations following from the considered 4-level system [69].

Since even contemporary works (not limited by available resolution as early experiments) comprising NMR measurements on liquid gallium [70–72] do not mention such splitting as observed here, validation measurements on the gallium sample without the pressure cell were carried out under ambient conditions. The validation experiments (the topmost panels of Fig. 1) yielded much narrower resonance lines (full width at half maximum of 7.2 ppm, no splitting) at frequencies higher by 207 ppm. This indicates an unexpected presence of local magnetic field inhomogeneity in the pressure cell. The mechanism of line splitting by field inhomogeneity is illustrated in a note in the Supplemental Material [67]. Nevertheless, the comparison of the data from the validation experiments allowed for correction of the NMR shifts measured on the liquid and solid phases of the sample in the pressure cell (see below).

TABLE I. Experimental NMR frequencies and (corrected) shifts Δ^{exp} [isotropic parts of frequency and shift $\Delta^{\mathrm{exp}}_{\mathrm{iso}}$ at 2.15(5) GPa].

Pressure	Isotope	Observed frequency (MHz)	Corrected frequency (MHz)	Shift Δ^{exp} ($\Delta^{\mathrm{exp}}_{\mathrm{iso}}$) (ppm)
Ambient (validation)	^{69}Ga	96.47241(1)		4486
	^{71}Ga	122.58012(1)		4485
Nearly ambient	^{69}Ga	96.453(1)		
	^{71}Ga	122.555(1)		
1.15(5) GPa	^{69}Ga	96.456(1)	96.475(10)	4517(80)
	^{71}Ga	122.559(1)	122.584(10)	4518(80)
2.15(5) GPa	^{71}Ga	122.605(2)	122.612(10)	4746(80)

The NMR shifts Δ^{exp} are summarized in Table I, while the spin-lattice (T_1) and spin-spin (T_2) relaxation times can be found in Table II. The spin-lattice relaxation is assumed to be composed of magnetic and quadrupole contributions, characterized by $T_{1\mathrm{m}}$ and $T_{1\mathrm{q}}$ times, respectively:

$$\begin{aligned} 1/T_1 &= 1/T_{1\mathrm{m}} + 1/T_{1\mathrm{q}}, \\ 1/T_{1\mathrm{m}} &= C_{\mathrm{m}}\gamma^2, \\ 1/T_{1\mathrm{q}} &= C_{\mathrm{q}}Q^2, \end{aligned} \tag{1}$$

where γ denotes the gyromagnetic ratio of resonating nuclei, Q stands for the quadrupole moment, while C_{m} and C_{q} are corresponding proportionality coefficients. Thus, the T_1 relaxation times of both gallium isotopes can be expressed by these relations:

$$\begin{aligned} 1/{}^{69}T_1 &= C_{\mathrm{m}}\,{}^{69}\gamma^2 + C_{\mathrm{q}}\,{}^{69}Q^2, \\ 1/{}^{71}T_1 &= C_{\mathrm{m}}\,{}^{71}\gamma^2 + C_{\mathrm{q}}\,{}^{71}Q^2. \end{aligned} \tag{2}$$

Solving the set of equations (2) allows for a separation of the magnetic and quadrupole contributions (Table II). Apparently, the magnetic part of relaxation is dominant in the liquid phase and is virtually the only relaxation mechanism in the solid phase [at 2.15(5) GPa, $^{71}T_1/^{69}T_1$ is equal within experimental error to $^{69}\gamma^2/^{71}\gamma^2$]. Under the assumption that Δ^{exp} is composed solely of the Knight shift K, the fulfillment of the Korringa relation [73] can be checked by comparing $T_{1\mathrm{m}}K^2T$ to

$$S_0 = \frac{\hbar}{4\pi k_{\mathrm{B}}}\frac{\gamma_e^2}{\gamma^2}, \tag{3}$$

where k_{B} is the Boltzmann constant and γ_e denotes the gyromagnetic ratio of electron (see the last column of Table II).

The most valuable information was obtained from a measurement of the dependence of the spectra on the orientation of the sample with respect to the magnetic field direction; see Fig. 2. The dependencies of the central transition frequency and frequency splitting between the satellites on the angle ϕ (Fig. 3) was fitted with this expression [74,75]:

$$f(\phi_i) = A_i + B_i\cos(2\phi_i) + C_i\sin(2\phi_i),\ \ i = x, y, z. \tag{4}$$

The coefficients A_i, B_i, and C_i found by the fit were then used to construct the following tensor $\mathbf{T}$ expressed in the pressure cell axis system:

$$\begin{aligned} T_{xx} &= (A_y - B_y + A_z + B_z)/2, \\ T_{yy} &= (A_z - B_z + A_x + B_x)/2, \\ T_{zz} &= (A_x - B_x + A_y + B_y)/2, \\ T_{xy} &= T_{yx} = -C_z, \\ T_{xz} &= T_{zx} = -C_y, \\ T_{yz} &= T_{zy} = -C_x. \end{aligned} \tag{5}$$

In the case of the central transition, the tensor $\mathbf{T}$ is usually related to the isotropic NMR shift Δ_{iso} and the traceless shift anisotropy tensor $\mathbf{\Delta}'_{\mathrm{ani}}$ in the pressure cell frame of reference:

$$\frac{\mathbf{T}^{\mathrm{CT}}}{{}^{71}f_{\mathrm{ref}}} = \Delta_{\mathrm{iso}} + \mathbf{\Delta}'_{\mathrm{ani}}. \tag{6}$$

However, the impact of the field inhomogeneity in the pressure cell exceeded the expected shift anisotropy (see below) by two orders of magnitude, so the resulting tensor $\mathbf{T}^{\mathrm{CT}}$ was treated as

$$\frac{\mathbf{T}^{\mathrm{CT}}}{{}^{71}f_{\mathrm{ref}}} = \Delta_{\mathrm{iso}} + X_{\mathrm{iso}} + \mathbf{X}'_{\mathrm{ani}}, \tag{7}$$

where X_{iso} and $\mathbf{X}'_{\mathrm{ani}}$ describe the isotropic and anisotropic effects of the field inhomogeneity, respectively. Although the NMR shift anisotropy was neglected, this approach in

TABLE II. Spin-lattice (T_1) and spin-spin (T_2) relaxation times, decomposition of T_1 into magnetic ($T_{1\mathrm{m}}$) and quadrupole ($T_{1\mathrm{q}}$) parts, and check of Korringa relation fulfillment.

Pressure	Isotope	T_1 (ms)	T_2 (ms)	$T_{1\mathrm{m}}$ (ms)	$T_{1\mathrm{q}}$ (ms)	$T_{1\mathrm{m}}K^2T/S_0$
Nearly ambient	^{69}Ga	0.696(10)	0.660(9)	0.943(14)	2.65(22)	1.24(2)
	^{71}Ga	0.538(5)	0.512(8)	0.584(9)	6.78(55)	
1.15(5) GPa	^{69}Ga	0.673(10)	0.630(28)	0.947(17)	2.32(18)	1.26(5)
	^{71}Ga	0.534(6)	0.503(16)	0.587(10)	5.94(47)	
2.15(5) GPa	^{69}Ga	0.825(30)	0.358(10)	$= T_1$		1.21(6)
	^{71}Ga	0.514(8)	0.122(3)	$= T_1$		1.22(5)

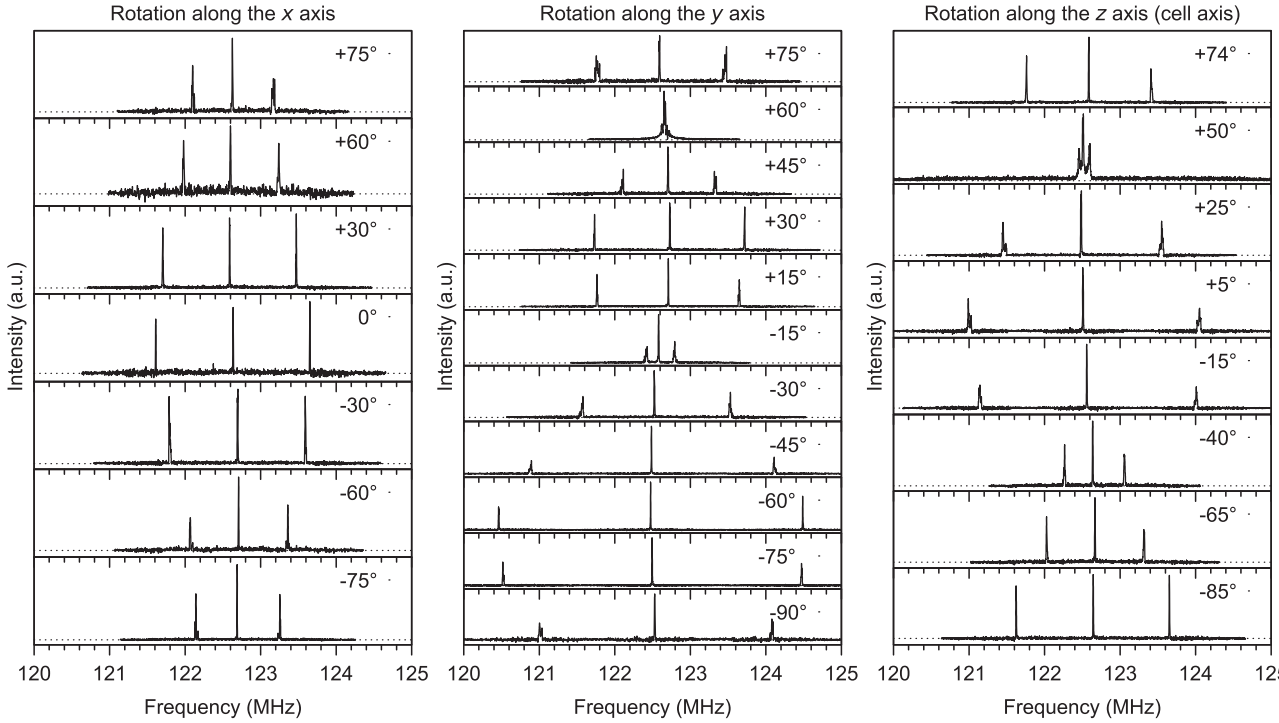

FIG. 2. The dependence of ^{71}Ga NMR spectra on the orientation of the sample with respect to the magnetic field direction measured at 2.15(5) GPa pressure. The rotation axis was perpendicular to the field direction.

combination with the validation measurements allowed for the determination of the isotropic NMR shift. The fit of the experimental data for 2.15(5) GPa yielded the tensor $\mathbf{X}'_{\text{ani}}$ and the sum $\Delta_{\text{iso}} + X_{\text{iso}}$. Since the X_{iso} and $\mathbf{X}'_{\text{ani}}$ parameters are the same for all the measurements in the cell (and the cell orientations $\vec{u}$ are known), comparison of the shift $\Delta^{\text{cell}}_{\text{ambient}}(\vec{u})$ at ambient pressure in the cell (NMR shift plus the shift due to the field inhomogeneity) with the NMR shift $\Delta^{\text{validation}}_{\text{ambient}}$ observed in the validation experiment provided the value of $X_{\text{iso}} = \Delta^{\text{cell}}_{\text{ambient}}(\vec{u}) - \Delta^{\text{validation}}_{\text{ambient}} - \vec{u}^{\text{T}}\mathbf{X}'_{\text{ani}}\vec{u}$. Then it was straightforward to obtain the isotropic NMR shift for the 2.15(5) GPa measurement, as well as to correct the NMR shift from the measurement at 1.15(5) GPa.

For the satellite transitions, the tensor $\mathbf{T}$ can be converted into the electric field gradient (EFG) tensor $\mathbf{V}'$ in the pressure cell coordinates:

$$\frac{h\mathbf{T}^{\text{sat}}}{e\,^{71}Q} = \mathbf{V}'. \tag{8}$$

The EFG tensor $\mathbf{V}'$ was brought to its canonical form $\mathbf{V}$, yielding $V_{zz} = 1.584 \times 10^{21}$ V m^{-2} and almost negligible asymmetry parameter $\eta = 0.011$.

III. CALCULATIONS

A. Calculation method

In order to better understand the experimental data and to confirm the particular phase of the obtained solid gallium, we carried out the *ab initio* calculations of the electronic structure of the Ga-III, Ga-II, and β-Ga phases, with the aim of extracting the hyperfine parameters as well as electronic populations. Density functional theory (DFT) calculations were performed using the full-potential augmented plane wave method as implemented in WIEN2k [76]. In all calculated structures (see Supplemental Material [67] for structural details) the radii of the gallium atomic spheres were 2.4 a.u. and the size of the basis $RK_{\text{MAX}} \sim 11$; the charge was Fourier-expanded up to $G_{\text{MAX}} = 14$ Ry$^{1/2}$ and PBE-GGA [77] was used as the exchange-correlation potential. For calculation of the spin-dipolar contribution to the hyperfine field, the spin-orbit coupling was considered within the atomic spheres using a second-variational method with the scalar-relativistic orbitals.

While the electric field gradient is readily available from the charge density, the NMR shift requires additional calculations to obtain the values of the diamagnetic and, in the case of metals, also paramagnetic shielding of the studied compounds, as well as of an appropriate reference compound. The method of calculating the NMR shielding, implemented in WIEN2k [78–80], is based on linear response theory. In the case of a diamagnetic contribution due to orbital moments of electrons, eigenvectors of the original and six slightly shifted (in the $\pm x$, $\pm y$, $\pm z$ directions) k meshes are used to compute the induced current and magnetic susceptibility, and the diamagnetic shielding is then calculated by integrating the induced current. In metallic systems a very dense k-point mesh and a suitable Fermi level smearing are needed. For the presented gallium structures the diamagnetic shieldings were well converged with 2.2×10^5 k points and Fermi broadening 5 mRy. The macroscopic magnetic susceptibility was impossible to converge even with mesh of 10^6 k points; however, its contribution to the shielding is on the order of a few ppm, and was thus neglected. To obtain the paramagnetic shielding is even more intricate and requires spin-polarized calculation to allow for interaction of electronic spins with

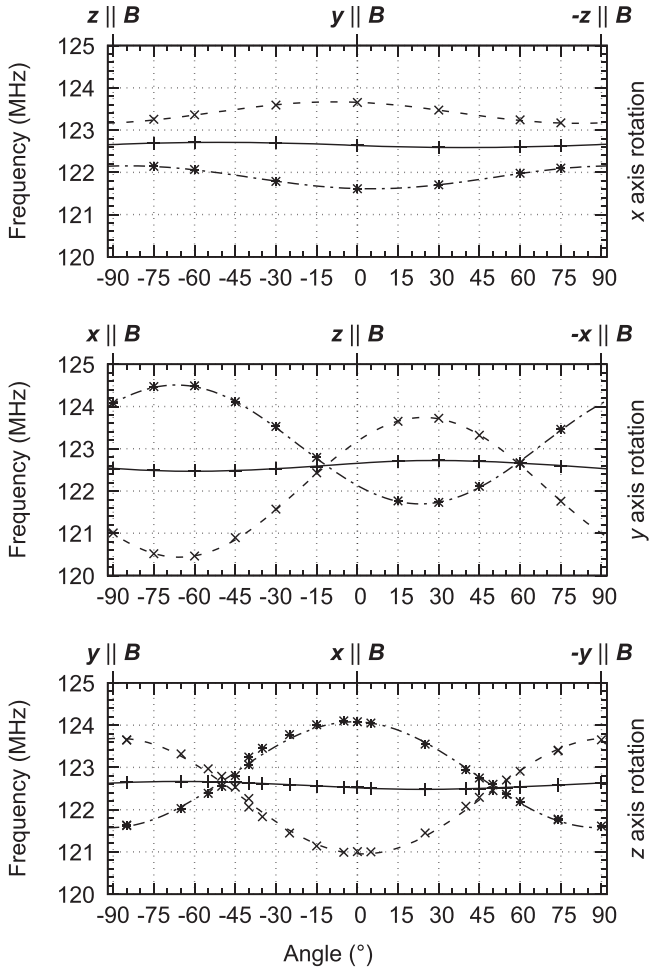

FIG. 3. The fit of the dependence of ^{71}Ga NMR resonance frequencies of the central (solid line) and satellite (dashed lines) transitions on the orientation of the sample with respect to the magnetic field direction measured at 2.15(5) GPa pressure. The rotation axes were perpendicular to the field direction $\boldsymbol{B}$.

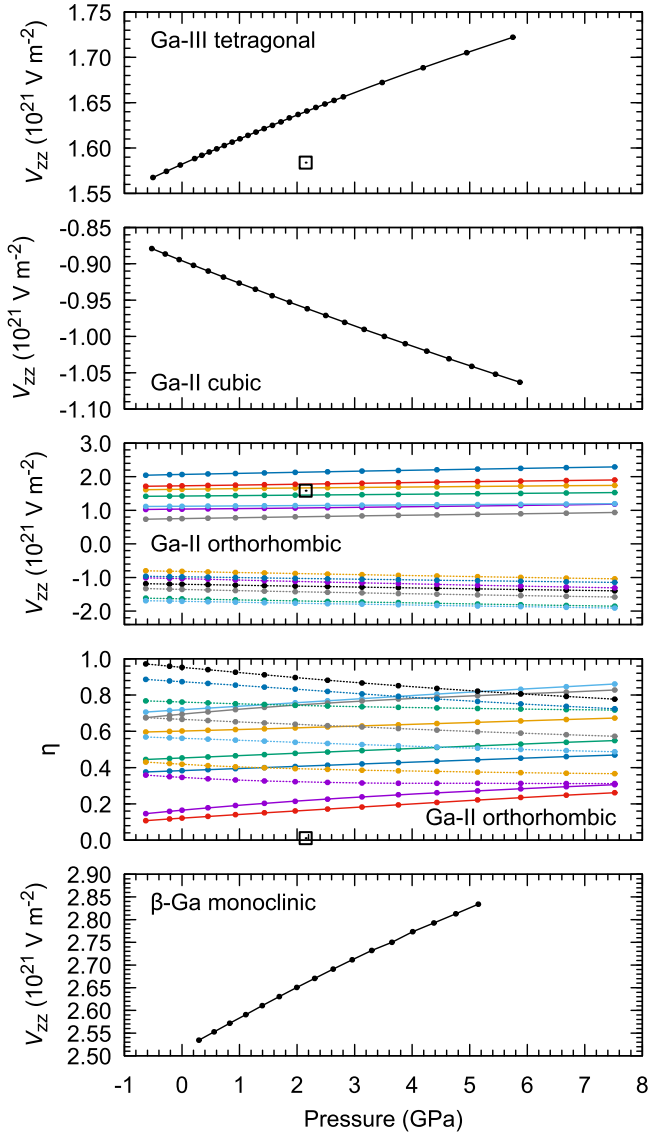

FIG. 4. Calculated pressure dependencies of EFG V_{zz} at Ga sites in the four considered Ga structures. Asymmetry parameter in the case of Ga-III and cubic Ga-II is $\eta = 0$, while it is $\eta = 0.37$ for β-Ga in the whole calculated range. For comparison, the square symbols denote the values measured on the investigated solid Ga phase. (The lines serve just as eye guides.)

explicitly applied magnetic field [81]. In order to estimate the contact field and spin dipolar field, we applied an interaction with external magnetic field of 100 T in the form of an appropriate energy shift $\pm\mu_B B_{\text{ext}}$ of the spin up/down exchange correlation potentials. The paramagnetic shielding was then evaluated from the contact and spin dipolar hyperfine fields as a response to the polarization by the external field. Again, the Fermi broadening of 5 mRy and very fine k-point meshes (10^6 k points) were required to provide a good convergence of the shielding in these metallic structures.

As an NMR reference, paramagnetic and diamagnetic shielding of cubic GaAs at 0 GPa was calculated analogously with the same parameters as for the metallic Ga compounds and assigned to the experimental shift 216(1) ppm [82]. Since the response to the external field was too small in the case of semiconducting GaAs, the applied field was increased to 1000 T to improve the precision.

Influence of various calculational parameters on calculated NMR shielding was tested and reasonable convergence (∼1 ppm) was achieved: especially the number of k points and Fermi level smearing but also other parameters related to NMR calculations were checked, such as the number of additional NMR local orbitals. The linearity of the response to the external field was found to be well assured in the range of about 30–2000 T. Higher fields already perturb the electronic structure, while calculations with lower values of external field suffer from insufficient numerical precision of the hyperfine field.

As a model to our NMR experiments under pressure, volume dependencies of the total energy were calculated and transformed to pressure dependencies via fitting by the Birch-Murnaghan equation of state [83]. The DFT calculations correspond to zero temperature while the experiments were performed at room temperature; therefore, we expect all calculated pressure dependencies to display a systematic

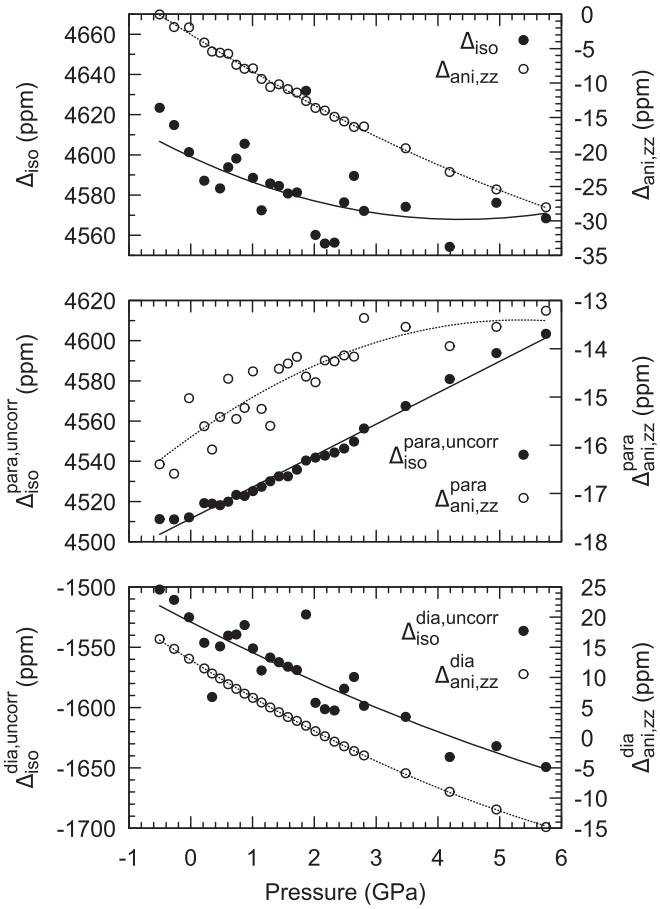

FIG. 5. Calculated pressure dependencies of isotropic and anisotropic parts of NMR shift in Ga-III structure; the total values corrected with respect to the GaAs reference, as well as uncorrected paramagnetic and diamagnetic contributions are shown. (The lines serve just as eye guides.)

shift due to thermal expansion, which roughly corresponds to negative pressure of about −0.3 GPa.

B. Calculation results

We focused mainly on the tetragonal Ga-III phase; however, the pressure dependencies of EFGs were calculated also for cubic Ga-II and monoclinic β-Ga; orthorhombic Ga-II was calculated with reduced size of the basis set and number of k points; see Fig. 4. In the case of cubic Ga-II and monoclinic β-Ga, the demanding calculations of NMR shieldings were performed for only one value of pressure (2.2 GPa; lower part

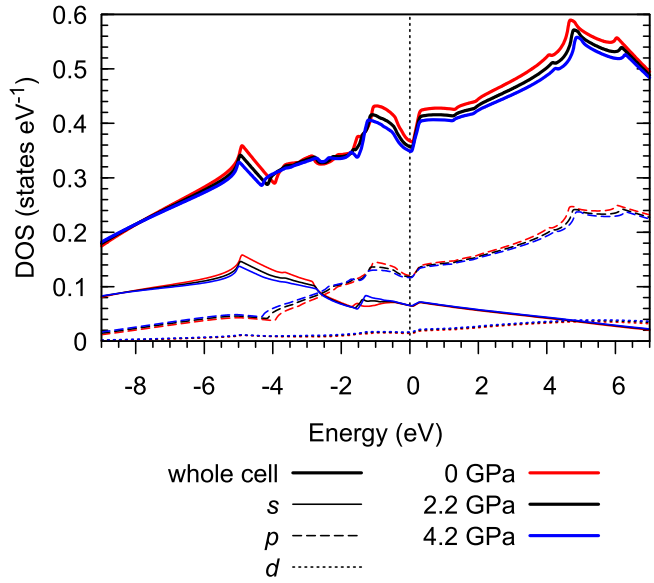

FIG. 6. Calculated total and partial densities of states in Ga-III structure at several pressures.

of Table VI). For each particular pressure, the atomic positions and remaining degrees of freedom in lattice parameters were optimized, with the exceptions of complex orthorhombic Ga-II structure and of monoclinic angle in β-Ga. In tetragonal Ga-III, special attention was paid to careful optimization of the c/a ratio, to which the values of EFG were sensitive. Detailed information about the calculated structures and changes during their optimization is provided in the Supplemental Material [67].

In all studied Ga structures, the dominant source of the EFG tensor originates from the pp contribution, which is slightly reduced by the dd contribution. As expected, with increasing pressure the interatomic distances shrink proportionally. The Ga $4p$ states thus become more populated and the corresponding elements of EFG increase in absolute value. The pressure dependence of the NMR shift in the Ga-III structure can be found in Fig. 5 and Table III. The anisotropy of the NMR shift was estimated by applying the interaction with external magnetic field in various crystallographic directions. Concerning the pressure variation of general electronic properties of the Ga-III phase, the plots of the density of states for several pressures can be found in Fig. 6, while the relation between electronic populations (Table IV) and hyperfine parameters can be assessed from Tables V and VI.

TABLE III. Calculated isotropic Δ_{iso} and anisotropic $\Delta_{ani,zz}$ parts of NMR shift of Ga-III phase at several pressures and their decomposition into diamagnetic (index ^{dia}) and paramagnetic (index ^{para}) contributions. The index ^{uncorr} denotes values not corrected with respect to the GaAs reference. The experimental value in the last row is provided for comparison.

Pressure	$\Delta_{iso}^{dia,uncorr}$ (ppm)	$\Delta_{iso}^{para,uncorr}$ (ppm)	Δ_{iso}^{uncorr} (ppm)	Δ_{iso} (ppm)	$\Delta_{ani,zz}^{dia}$ (ppm)	$\Delta_{ani,zz}^{para}$ (ppm)	$\Delta_{ani,zz}$ (ppm)
0 GPa	−1525	4512	2987	4601	13	−15	−2
2.2 GPa	−1601	4543	2942	4556	0	−14	−14
4.2 GPa	−1641	4581	2940	4554	−9	−14	−23
2.15(5) GPa experiment				4746(80)			

TABLE IV. Calculated electronic populations of Ga-III phase at several pressures (corrected for pressure-induced changes of interstitial volume).

Pressure	s	p	d	f	p_z	$p_x + p_y$	d_{z^2}	d_{xy}	$d_{x^2-y^2}$	$d_{xz} + d_{yz}$
0 GPa	1.030	0.566	9.954	0.007	0.177	0.389	1.989	1.987	1.994	3.984
2.2 GPa	1.024	0.593	9.949	0.008	0.186	0.408	1.988	1.986	1.993	3.982
4.2 GPa	1.019	0.616	9.946	0.009	0.193	0.423	1.987	1.984	1.993	3.981

IV. DISCUSSION

The experimental NMR shifts of liquid gallium at ambient conditions reported in this work are comparable to the shifts published in older works: 4528 ppm [48] and 4490 ppm [41]. The relaxation times under the same conditions match very well the spin-lattice relaxation data in Ref. [48] and they are also comparable to the spin-lattice and spin-spin relaxation times of the sample with the longest relaxations in Ref. [41], while they are about 5% shorter compared with the spin-lattice relaxations reported in Ref. [44]. The spin-lattice relaxation times in the liquid and solid phases exceed the expectations based on the Korringa relation by 21% to 26%, indicating the presence of electronic correlations.

The verification of the gallium solid phase obtained in the experiment takes advantage of the quadrupole splitting. The calculated EFG parameters of the metastable monoclinic β-Ga phase are in reasonable agreement with published experimental data [$V_{zz} = 2.400(2) \times 10^{21}$ V m^{-2}, $\eta = 0.312(5)$ at 242 K] [60] and they clearly differ from the values measured in this work. Calculations of the cubic Ga-II structure also yielded V_{zz} noticeably different from our measurement, whereas the complex orthorhombic Ga-II phase with 14 independent crystal sites of Ga ions would apparently give rise to a complicated structure of spectra which is not the case [1]. On the other hand, the axially symmetric EFG tensor found in our experiment corresponds well to a symmetry of the tetragonal Ga-III phase and comparison of the measured value of $V_{zz} = 1.584 \times 10^{21}$ V m^{-2} at 2.15(5) GPa with the EFG calculated for this structure ($V_{zz} = 1.641 \times 10^{21}$ V m^{-2} at 2.2 GPa) clearly yields Ga-III as the best match.

The experimentally observed isotropic part of the NMR shift in the solid phase $\Delta_{\text{iso}}^{\text{exp}} = 4746(80)$ ppm at 2.15(5) GPa reasonably matches the value calculated for the Ga-III structure ($\Delta_{\text{iso}} = 4556$ ppm at 2.2 GPa). The local perturbation of field homogeneity in the pressure cell, which led to the line splitting, reduced the precision [2] of the measured isotropic NMR shifts and completely hindered the determination of the NMR shift anisotropy. It was caused probably by the presence of some tiny magnetic impurity introduced perhaps in the cell chassis during machining or in the gasket when carving the channels for the RF coil leads; alternatively, a small content of magnetic impurities in the three set screws for fine alignment of the anvils could be also a possible explanation. We should also note that due to the field inhomogeneity, closer examination of satellite signals of the solid phase revealed in some orientations rather complex line patterns.

The DFT calculations identified the p electrons as the primary source of the EFG in all calculated gallium metal phases. The differences in calculated EFGs between the Ga structures correspond to a character of the local structure. The gallium site with the highest local symmetry (-4) is in the cubic Ga-II structure and possesses the lowest value of EFG. Similarly, in the Ga-III structure, which also lacks any free internal structural parameters, the EFG appears due to tetragonal deformation that makes the local symmetry $4/mmm$; otherwise, for $c/a = \sqrt{2}$, the structure would be cubic Fm-3m with local symmetry of Ga site m-3m and zero EFG. Gallium in β-Ga has the highest EFG values among the studied compounds, which corresponds to low local symmetry (point group 2).

Concerning the origin of the NMR shift in Ga-III, as well as in cubic Ga-II and β-Ga, Table VI reveals that the Fermi contact contribution presents a dominant part of the shift, while the dipolar contributions of the p shell are much smaller and those of the d shell are even weaker. The diamagnetic shift

[1] Unfortunately, comparison with the NMR experiments on the Ga-II phase in Ref. [62] is not possible since only central line data are reported therein.

[2] Since the pressure cell had to be removed from the holder for every pressure increase, the orientation uncertainty of $\pm 3^\circ$ had to be taken into account in the compensation for the field inhomogeneity impact on the resulting NMR shifts.

TABLE V. The decomposition of calculated EFG of Ga-III phase at several pressures. The experimental value in the last row is provided for comparison.

Pressure	pp (10^{21} V m^{-2})	sd (10^{21} V m^{-2})	dd (10^{21} V m^{-2})	pf (10^{21} V m^{-2})	ff (10^{21} V m^{-2})	total (10^{21} V m^{-2})	V_{zz} (including interstitial) (10^{21} V m^{-2})
0 GPa	1.673	0.005	−0.087	0.005	0.000	1.596	1.581
2.2 GPa	1.746	0.007	−0.099	0.005	0.000	1.658	1.641
4.2 GPa	1.806	0.007	−0.107	0.005	0.000	1.710	1.689
2.15(5) GPa experiment							1.584

TABLE VI. The decomposition of calculated NMR shifts Δ of Ga-III phase for magnetic field along the *c* and *a* axes at several pressures and of GaAs used as a reference compound. The calculated data for cubic Ga-II and *β*-Ga phases for magnetic field along the *c* axis are provided for comparison. ($\Delta^{\text{dia,uncorr}}$ corresponds to diamagnetic part obtained as chemical shielding and the other columns form together paramagnetic part $\Delta^{\text{para,uncorr}}$: contact stands for Fermi contact contribution, while dip denotes spin-dipolar contribution of particular shell.) (The index $^{\text{uncorr}}$ denotes values not corrected with respect to the GaAs reference.)

			$\Delta^{\text{para,uncorr}}$				Total shift		
Structure	Pressure	$\Delta^{\text{dia,uncorr}}$ (ppm)	contact (ppm)	dip *s* (ppm)	dip *p* (ppm)	dip *d* (ppm)	Δ^{uncorr} (ppm)	Δ (ppm)	Field direction
Ga-III	0 GPa	−1512	4517	0	−20	1	2987	4601	*c* axis
	2.2 GPa	−1601	4547	0	−18	1	2929	4543	*c* axis
	4.2 GPa	−1650	4584	0	−18	1	2917	4532	*c* axis
Ga-III	0 GPa	−1532	4511	0	8	−1	2987	4602	*a* axis
	2.2 GPa	−1601	4543	0	8	−1	2949	4563	*a* axis
	4.2 GPa	−1637	4580	0	8	−1	2950	4565	*a* axis
GaAs	0 GPa	−1344	−55	0	0	0	−1398	216	
Ga-II cubic	2.2 GPa	−1537	4135	0	5	0	2603	4217	*c* axis
β-Ga	2.2 GPa	−1367	3748	0	33	−3	2412	4026	*c* axis

contribution is to a large extent canceled by the correction using the GaAs reference. The dipolar moments of *p* electrons are a major source of the paramagnetic shift anisotropy.

Calculated total and partial densities of states in the Ga-III structure (Fig. 6) correspond to the metallic, free-electron character of the Ga-III electronic structure. The shape of the displayed DOS does not change much within the considered pressure range and is in good agreement with calculated data published in Ref. [26].

V. CONCLUSION

We carried out ^{69}Ga and ^{71}Ga NMR measurements on liquid and solid gallium metal under pressure. The *ab initio* calculations were employed as a complement of the measurements, allowing for verification of the particular phase of solid gallium obtained in the experiment and for deeper insight into the hyperfine and electronic properties. While our experimental data (NMR shift and relaxation times) on the liquid phase fit the current picture of this metal, the investigation of the solid phase presents an experimental and theoretical study of the hyperfine parameters of the Ga-III phase. The EFG and NMR shift of Ga-III were both measured and calculated, yielding reasonable agreement of the EFG parameters and of the isotropic components of the NMR shifts. The experimentally observed line splitting was ascribed to magnetic field inhomogeneities in the pressure cell, while the additional shift caused by these inhomogeneities was subtracted from the resulting NMR shift parameters. The hyperfine parameters were interpreted in terms of electronic structure, revealing the dominant contribution of Fermi contact interaction to the NMR shift and the significant role of *p* electrons in the shift anisotropy and EFG. Further, the calculations of the pressure dependence of the EFG parameters of complex orthorhombic Ga-II structure prepare the ground for prospective experimental study.

ACKNOWLEDGMENTS

The experimental part of this work was supported by Deutsche Forschungsgemeinschaft within Project No. 252360796 (HA 1893/12-1), "Metals under extreme conditions." Computational resources were provided by CESNET LM2015042 and CERIT Scientific Cloud LM2015085, provided under the program "Projects of Large Research, Development, and Innovations Infrastructures."

[1] L. Bosio, J. Chem. Phys. **68**, 1221 (1978).
[2] L. Comez, A. Di Cicco, J. P. Itié, and A. Polian, Phys. Rev. B **65**, 014114 (2001).
[3] P. W. Bridgman, Phys. Rev. **48**, 893 (1935).
[4] C. E. Weir, G. J. Piermarini, and S. Block, J. Chem. Phys. **54**, 2768 (1971).
[5] L. Bosio, A. Defrain, H. Curien, and A. Rimsky, Acta Crystallogr. B **25**, 995 (1969).
[6] A. Jayaraman, W. Klement, Jr., R. C. Newton, and G. C. Kennedy, J. Phys. Chem. Solids **24**, 7 (1963).
[7] O. Schulte and W. B. Holzapfel, Phys. Rev. B **55**, 8122 (1997).
[8] O. Degtyareva, M. I. McMahon, D. R. Allan, and R. J. Nelmes, Phys. Rev. Lett. **93**, 205502 (2004).
[9] K. Takemura, K. Kobayashi, and M. Arai, Phys. Rev. B **58**, 2482 (1998).
[10] O. Schulte, A. Nikolaenko, and W. B. Holzapfel, High Pressure Res. **6**, 169 (1991).
[11] A. G. Lyapin, E. L. Gromnitskaya, O. F. Yagafarov, O. V. Stal'gorova, and V. V. Brazhkin, J. Exp. Theor. Phys. **107**, 818 (2008).
[12] E. L. Gromnitskaya, O. F. Yagafarov, O. V. Stalgorova, V. V. Brazhkin, and A. G. Lyapin, Phys. Rev. Lett. **98**, 165503 (2007).
[13] L. Bosio, R. Cortes, J. R. D. Copley, W. D. Teuchert, and J. Lefebvre, J. Phys. F: Metal Phys. **11**, 2261 (1981).
[14] V. M. Nield, R. L. McGreevy, and M. G. Tucker, J. Phys.: Condens. Matter **10**, 3293 (1998).

[15] D. A. Jackson, Phys. Rev. **103**, 1738 (1956).
[16] R. H. Hammond and W. D. Knight, Phys. Rev. **120**, 762 (1960).
[17] E. J. Unterhorst, V. Müller, and G. Schanz, Phys. Status Solidi B **84**, K53 (1977).
[18] B. P. Panda and N. C. Mohapatra, Pramana J. Phys. **61**, 1151 (2003).
[19] O. N. Bakharev, D. Bono, H. B. Brom, A. Schnepf, H. Schnöckel, and L. J. de Jongh, Phys. Rev. Lett. **96**, 117002 (2006).
[20] F. Greuter and P. Oelhafen, Z. Phys. B **34**, 123 (1979).
[21] Ch. Splx-sol-plxondergaard, Ch. Schultz, S. Agergaard, H. Li, Z. Li, S. V. Hoffmann, Ch. Grütter, J. H. Bilgram, and Ph. Hofmann, Phys. Rev. B **67**, 205105 (2003).
[22] H. Schnöckel, Chem. Rev. **110**, 4125 (2010).
[23] J. E. Inglesfield, J. Phys. C (Proc. Phys. Soc.) **1**, 1337 (1968).
[24] M. Bernasconi, G. L. Chiarotti, and E. Tosatti, Phys. Rev. B **52**, 9988 (1995).
[25] M. I. Baskes, S. P. Chen, and F. J. Cherne, Phys. Rev. B **66**, 104107 (2002).
[26] E. Voloshina, K. Rosciszewski, and B. Paulus, Phys. Rev. B **79**, 045113 (2009).
[27] Z. Li and J. S. Tse, Phys. Rev. B **62**, 9900 (2000).
[28] M. de Koning, A. Antonelli, and D. A. C. Jara, Phys. Rev. B **80**, 045209 (2009).
[29] M. Bernasconi, G. L. Chiarotti, and E. Tosatti, Phys. Rev. Lett. **70**, 3295 (1993).
[30] B. K. Acharya and N. C. Mohapatra, Hyperfine Interact. **116**, 179 (1998).
[31] B. P. Panda and N. C. Mohapatra, Physica B **344**, 108 (2004).
[32] B. K. Acharya and N. C. Mohapatra, Pramana J. Phys. **43**, 391 (1994).
[33] K. W. Lodge, J. Phys. F **8**, 447 (1978).
[34] J. D. Stroudt and M. J. Stott, J. Phys. F **5**, 1667 (1975).
[35] S. Chacko, K. Joshi, D. G. Kanhere, and S. A. Blundell, Phys. Rev. Lett. **92**, 135506 (2004).
[36] X. G. Gong, G. L. Chiarotti, M. Parrinello, and E. Tosatti, Phys. Rev. B **43**, 14277 (1991).
[37] Z. Y. Zhu, Y. C. Cheng, and U. Schwingenschlögl, J. Phys.: Condens. Matter **23**, 475502 (2011).
[38] Z. Zhu, X. Wang, and U. Schwingenschlögl, Appl. Phys. Lett. **98**, 241902 (2011).
[39] A. S. Mikhaylushkin, S. I. Simak, B. Johansson, and U. Häussermann, J. Phys. Chem. Solids **67**, 2132 (2006).
[40] I. Spagnolatti and M. Bernasconia, Eur. Phys. J. B **36**, 87 (2003).
[41] D. A. Cornell, Phys. Rev. **153**, 208 (1967).
[42] K. Suzuki and O. Uemura, J. Phys. Chem. Solids **32**, 1801 (1971).
[43] D. Hechtfischer, R. Karcher, and K. Lüders, J. Phys. F **3**, 2021 (1973).
[44] G. Cartledge, R. L. Havill, and J. M. Titman, J. Phys. F **3**, 213 (1973).
[45] W. W. Warren, Jr., Phys. Rev. A **10**, 657 (1974).
[46] N. C. Halder, J. Magn. Reson. **15**, 339 (1974).
[47] N. C. Halder, Phys. Rev. B **10**, 2333 (1974).
[48] A. L. Kerlin and W. G. Clark, Phys. Rev. B **12**, 3533 (1975).
[49] N. C. Halder, J. Magn. Reson. **22**, 33 (1976).
[50] R. H. Hammond, E. G. Wiener, and G. M. Kelly, Phys. Rev. **143**, 275 (1966).
[51] J. Y. Hwang, P. C. Canepa, and T. A. Scott, J. Phys. Chem. Solids **38**, 1403 (1977).
[52] M. I. Valič and D. Llewelyn Williams, J. Phys. Chem. Solids **30**, 2337 (1969).
[53] M. I. Valič and D. Llewelyn Williams, J. Phys. Chem. Solids **33**, 1583 (1972).
[54] M. I. Valič, S. N. Sharma, and D. Llewelyn Williams, Phys. Lett. A **26**, 528 (1968).
[55] M. I. Valič and D. Llewelyn Williams, Solid State Commun. **8**, 1455 (1970).
[56] M. I. Valič, Ph.D. thesis, University of British Columbia, 1970.
[57] M. Huebner, Th. Wagner, S. Götz, and G. Eska, Physica B **210**, 484 (1995).
[58] S. L. Segel and J. D. Stroud, J. Phys. F **5**, 1986 (1975).
[59] R. J. C. Brown and S. Segel, J. Phys. F **5**, 1073 (1975).
[60] J. D. Stroud and S. L. Segel, J. Phys. F **5**, 1981 (1975).
[61] S. L. Segel, R. D. Heyding, and E. F. W. Seymour, Phys. Rev. Lett. **28**, 970 (1972).
[62] T. Meier, Annu. Rep. NMR Spectrosc. **93**, 1 (2018); Ph.D. thesis, University of Leipzig, 2016.
[63] T. Meier, T. Herzig, and J. Haase, Rev. Sci. Instrum. **85**, 043903 (2014).
[64] H. K. Mao, P. M. Bell, J. W. Shaner, and D. J. Steinberg, J. Appl. Phys. **49**, 3276 (1978).
[65] P. M. Bell, J. A. Xu, and H. K. Mao, in *Shock Waves in Condensed Matter* (Springer US, Boston, MA, 1986), pp. 125–130.
[66] R. J. Hemley, C. S. Zha, A. P. Jephcoat, H. K. Mao, L. W. Finger, and D. E. Cox, Phys. Rev. B **39**, 11820 (1989).
[67] See Supplemental Material at http://link.aps.org/supplemental/10.1103/PhysRevB.99.125121 for additional notes, table, figures, and files.
[68] P. Pyykkö, Mol. Phys. **99**, 1617 (2001).
[69] J. Haase, N. J. Curro, R. Stern, and C. P. Slichter, Phys. Rev. Lett. **81**, 1489 (1998).
[70] E. Shabanova, E. V. Charnaya, K. Schaumburg, and Yu. A. Kumzerov, Physica B **229**, 268 (1997).
[71] E. V. Charnaya, T. Loeser, D. Michel, C. Tien, D. Yaskov, and Yu. A. Kumzerov, Phys. Rev. Lett. **88**, 097602 (2002).
[72] E. V. Charnaya, D. Michel, C. Tien, Yu. A. Kumzerov, and D. Yaskov, J. Phys.: Condens. Matter **15**, 5469 (2003).
[73] J. Korringa, Physica **16**, 601 (1950).
[74] M. A. Kennedy and P. D. Ellis, Concept. Magnetic Res. **1**, 109 (1989).
[75] A. J. Woo, Bull. Korean Chem. Soc. **20**, 1205 (1999).
[76] P. Blaha, K. Schwarz, G. K. H. Madsen, D. Kvasnicka, and J. Luitz, *WIEN2k, An Augmented Plane Wave + Local Orbitals Program for Calculating Crystal Properties* (Karlheinz Schwarz, Techn. Universität Wien, Austria, 2001).
[77] J. P. Perdew, K. Burke, and M. Ernzerhof, Phys. Rev. Lett. **77**, 3865 (1996).
[78] R. Laskowski and P. Blaha, Phys. Rev. B **85**, 035132 (2012).
[79] R. Laskowski and P. Blaha, Phys. Rev. B **85**, 245117 (2012).
[80] R. Laskowski and P. Blaha, Phys. Rev. B **89**, 014402 (2014).
[81] R. Laskowski, K. Khoo, F. Haarmann, and P. Blaha, J. Phys. Chem. C **121**, 753 (2017).
[82] O. H. Han, H. K. C. Timken, and E. Oldfield, J. Chem. Phys. **89**, 6046 (1988).
[83] F. Birch, Phys. Rev. **71**, 809 (1947).